

Vorticity Propagation for Spin-up and Spin-down in a Rotating Tank

Frieder Kaiser^{1,*}, Tobias Wahl¹, Davide Gatti¹, David E. Rival², Jochen Kriegseis¹

1: Institute of Fluid Mechanics, Karlsruhe Institute of Technology, Germany

2: Department of Mechanical and Materials Engineering, Queen's University, Canada

* Correspondent author: frieder.kaiser@kit.edu

Keywords: PIV, vorticity, vortex flows, boundary layers, transient flow

ABSTRACT

This study focuses on the formation of a boundary layer and the corresponding behaviour of vorticity during impulsive spin-up and spin-down motions of a rotating tank. In particular, the difference between the dispersion of vorticity in a quiescent flow and in a flow with an established pressure gradient and a counter-oriented vorticity is of interest. The rotating tank was accelerated from rest to a rotational speed (spin-up) until the flow settled into a solid-body rotation (SBR) and afterwards stopped completely, until eventually the initial quiescent state is reached (spin-down). Four rotational speeds were investigated for spin-up and spin-down and the developing flow field was analysed by means of planar and stereo particle image velocimetry (PIV).

1. Motivation

Even though vorticity and vortical structures have been studied extensively in the last decades, there still remain open yet fundamental questions on the (limited) invariance of initial and boundary conditions on the generation, reorientation and annihilation of vorticity. This work thus strives to continue on with the experiments regarding the influence of initial conditions on vorticity and its formation (Kriegseis et al., 2013). Here the purpose is to explore the sudden interaction and subsequent evolution of opposite-signed vorticity layers under similar yet distinct initial conditions. To provide a deep insight into the scaling and behaviour of rapid vorticity annihilation processes, rotating facilities are either started from rest (irrotational initial condition) or stopped from spinning (rotational core initial condition) at identical characteristic time and length scales (see Figure 1). It is hypothesized that the diffusion of rotating-axis-oriented vorticity will move radially inwards, analogous to the behaviour of an inverse Lamb-Oseen vortex (with the radial position of the rotational front proportional to $\sqrt{\nu t}$). For the case of rotational initial conditions, it is expected that the opposite-signed vorticity generated at the wall will act to annihilate vorticity across an interface also moving inwards radially, again at a diffusion-limited time scale. The differences between the two cases, where the clash of vorticity of different signs (spin-down) is compared to simple diffusion into a resting fluid (spin-up)

might lead to a deeper understanding of vorticity in general. Another question of interest is the scaling effect for large Reynolds numbers $Re = \Omega R^2/\nu$ in both cases. Here, Ω is the final angular velocity of the tank in the steady state and R its radius. The larger gradients might influence the timescale of vorticity propagation. To investigate the problem of vorticity at high Reynolds numbers experiments were performed in a rotating tank and the flow was measured by applying PIV.

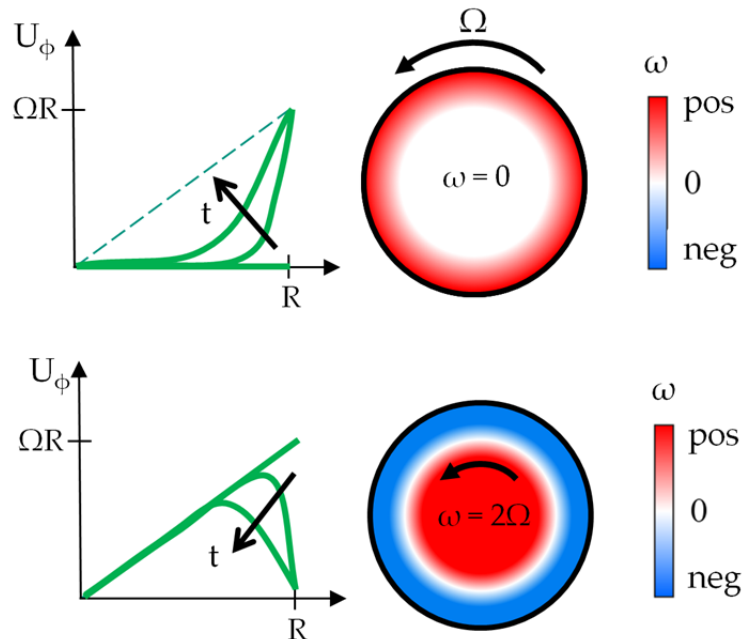


Fig. 1 Outline of the two cases: azimuthal velocity profile and vorticity during spin-up (top) and spin-down (bottom)

In contrast to the two-dimensional cases presented in Figure 1, an experimental implementation in a rotating tank is bounded by a bottom wall and a free upper surface. This adds additional complexity to the flow observable in experiments, which might complicate the extraction of answers to the fundamental questions on the nature of propagating vorticity.

The discovery of the Ekman layer in 1905 paved the way for the theoretical work of Greenspan and Howard (1963) on the spin-up and spin-down behaviour of tanks. An Ekman layer occurs at the end-walls as soon as the angular velocity of the tank is modified and leads to convective mixing, characterised by the Ekman number $E = \nu/(\Omega H^2)$, where H is the height of the tank. Early analytical studies were limited to small changes of the angular frequency in order to allow linearized solutions. Wedemeyer (1964) extended the theory to medium Rossby numbers $Ro = \Delta\Omega/\Omega$, where non-linear effects come into play. Benton and Clark (1974) and Duck and Foster (2001) provide detailed reviews on the analytical approaches. Obviously, for cylinders with large aspects ratios H/R , the influence of the end-walls and thus the effect of Ekman

pumping decreases. Furthermore, an experimental setup with a free surface also reduces the convective mixing caused by Ekman pumping, as the surface deformation buffers the convection; see e.g. O'Donnell and Linden (1991) and Cederlöf (1988). Besides the influences of the end walls, instabilities caused by an imbalance of pressure gradient and centrifugal forces can occur at the side walls of rotating flows. Rayleigh (1917) stated that for inviscid fluids a radial decrease of the circulation's magnitude is a sufficient condition for inviscid instabilities

$$\frac{d(\Gamma^2)}{dr} < 0.$$

However, the stabilizing effect of viscosity causes the onset of the instabilities to appear only beyond certain values of the Reynolds number (Taylor, 1923). In rotating cylinders with large aspect ratios Euteneuer (1972) investigated such instabilities resulting in counter-rotating vortices in streamwise direction at the side walls (called Görtler vortices; see Saric (1994)).

The propagation and annihilation of vorticity and the influences of end-wall effects, which make the extraction of the fundamental question more difficult, is part of the present work. In the case of small Reynolds numbers this study is further supported by numerical data, which allowed the manipulation of initial and boundary conditions and the elimination of end-wall effects.

2. Experimental Procedure



Fig. 2 Experimental setup: (1) rotating tank, (2) Nd:YAG laser with (3) light sheet optic, (4) trigger unit, (5) base framework with camera and drive system

The experiments are carried out in rotating tank made from acrylic glass to ensure optimal optical access (see Figure 2). It has an inner diameter of $2R = 0.49$ m and is filled with water to a level of $H = 0.49$ m. This results in an open surface configuration with an aspect ratio of $H/R = 2$. The rotation of the tank is driven by a low-g geared 12 V DC motor mounted below the tank. The motor's rotor signal is fed through a PID-feedback loop, which controls the provided current. This ensured a fast and smooth spin-up and a constant spin-rate to establish the required SBR in a variable range of frequencies from 0.5 Hz to 1.25 Hz. However, while an impulsive start should ideally occur instantly, the motor accelerated to the final speed in one to four rotations (depending on the final angular frequency). Additionally, triggered by a light barrier, a short circuit of the motor was implemented to ensure a fast and reproducible spin-down of the tank. The rotation axis of the tank and the drive shaft were carefully aligned prior to the experiments to ensure a mere rotary motion and a vertical position of the rotation axis.

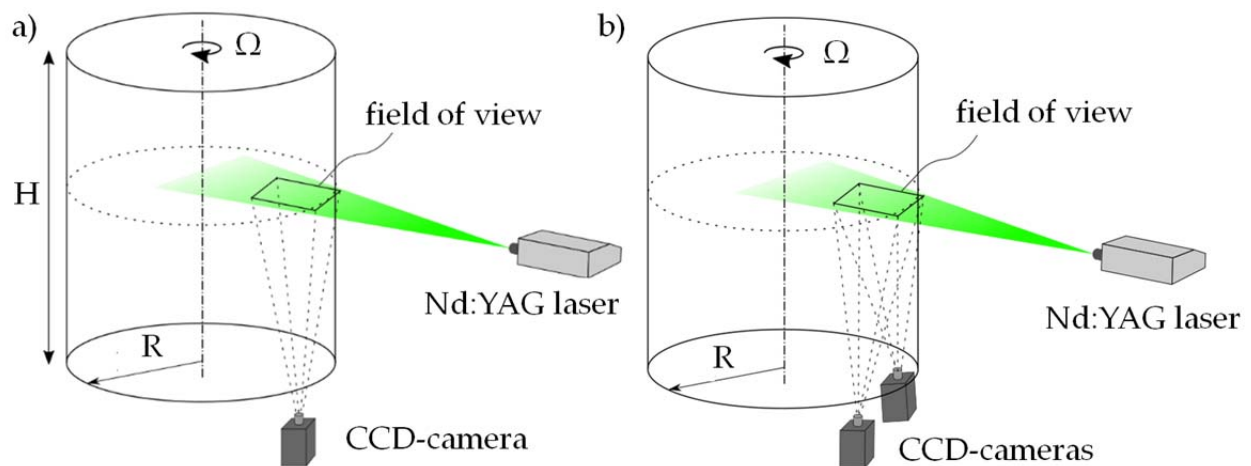


Fig. 3 (a) Sketch of the 2D2C-setup, (b) Sketch of the 2D3C-setup

Two different PIV setups were used during this study. The majority of the measurements were performed in the standard single camera setup sketched in Figure 3(a), measuring the two in-plane velocity components. Images were recorded with double-frame camera (PCO Pixefly) and a 50 mm f/1.4D Nikon Nikkor lens. To avoid image deformation due to free surface effects, the camera was mounted below the tank. This placed restrictions on the maximum imaging distance, so only a partial segment (90×60 mm) of the measurement plane could be captured. At a maximum camera resolution of 1392×1040 pixels, a spatial resolution of ~ 15 px/mm was achieved. A dual pulsed Nd:YAG laser (Quantel Evergreen 70) was used for flow illumination. A pulse energy of 20 mJ/pulse ensured sufficient illumination at a f-number of 8. The focal point of the optical system was placed near the axis of rotation to provide uniform lighting across the

whole field of view (FOV). The laser sheet had an average thickness of 2 mm, which guaranteed minimal particle loss due to out-of-plane movement. Pulse distances ranged from 500 μs to 2000 μs , depending on the rotational speed of the tank and were calculated to result in a maximum of 20 px displacement based on the rotational velocity at the wall. This large displacement was necessary as high velocity gradients occurred in both spin-ups and spin-downs and even minimal movements had to be captured accurately. Rectangular interrogation-areas (96×32 px, 75% and 50% overlap, respectively) were used. The long axis was in the tangential flow direction to accommodate the high velocity flow and reduce significant in-plane losses (Raffel et al., 2007).

Additionally, to check on potential out-of-plane velocities, a stereo setup was implemented (see Figure 3(b)). To minimize distortions, the optical access of the second camera was also realised through the bottom of the tank. The limited spatial extend of the bottom wall led to a small angle of 32° between the two cameras, reducing the quality of the stereo evaluation. However, as this setup pointed towards a qualitative evaluation of the out of plane component, the suboptimal camera positions were considered to be acceptable.

Polyamid powder (Polyamid 12, density 1.016 g/cm³, median diameter 20 μm) was used as tracers because it is neutrally buoyant in water. This is of paramount importance, since it avoids agglomeration and drastic settling before spin-ups and between different measurement series. The camera and laser system were operated in a phase-locked mode at up to ten frames per second (depending on the rotational speed) and 1000 images were recorded for each case. In addition to each spin-up and spin-down case, the "steady" flow was recorded with a fully developed SBR. As transient situations are difficult to evaluate statistically, the steady case was used as a reference and quality control for the flow and measurement system. The waiting period to achieve a fully developed SBR was 15 min to 30 min and was confirmed visually by observing particle behaviour seeded on the surface.

Raw images were pre-processed with calibration and dewarping to get an accurate absolute position and in case of the stereo setup to compensate distortion. The calibration target was first aligned with the laser sheet and two corners were positioned at the inner wall of the rotating tank. Thus, the centerline of the calibration target would always point towards the axis of rotation and could be used as a reference. A multi-grid/multi-pass correlation scheme with an initial grid-size of 192×192 px was used for the actual image processing. Due to the changing flow field, only a normalized median test (threshold 3) was used to detect

outliers (Westerweel and Scarano, 2005). Overall less than 0.5% outliers were detected and had to be corrected with secondary correlation peaks or interpolation methods. Finally, the Cartesian coordinate system was converted to a cylindrical system.

3. Accuracy, Reproducibility and Dependency on the Axial Position

Before the experimental data is discussed, this section provides an overview of the measure taken to evaluate the measurement quality. To ensure comparability between the different cases processed in this study, all following results are normalised by $r^* = \frac{r}{R}$, $t^* = \Omega t$, $U_\phi^* = \frac{U_\phi}{\Omega R}$, $U_r^* = \frac{U_r}{\Omega R}$, $U_z^* = \frac{U_z}{\Omega R}$, $\omega^* = \frac{\omega}{2\Omega}$, where r is the radial position, t is the time, ω is the vorticity in the $r - \theta -$ plane and U_ϕ , U_r and U_z are the velocities in azimuthal, radial and axial direction.

Transient problems are inherently difficult to evaluate for statistical significance. To show the accuracy of the experimental setup, the fully developed SBR, which forms the initial condition for the spin-down experiments, was used to get statistical information. Figure 4(a) shows good agreement of the measured azimuthal velocities to the theoretical values as the deviations are within 2%. To further ensure the reliability of the measurements, a convergence plot is used. The standard deviations σ of the mean value of the azimuthal velocity were calculated over time at five randomly chosen points, uniformly distributed in the FOV. Normalized by the theoretical azimuthal velocity at their respective position, they converge to very small values (≈ 0.003) at around $N=100$ samples, which is a direct statement of the accuracy of the measurement (Figure 4(b)).

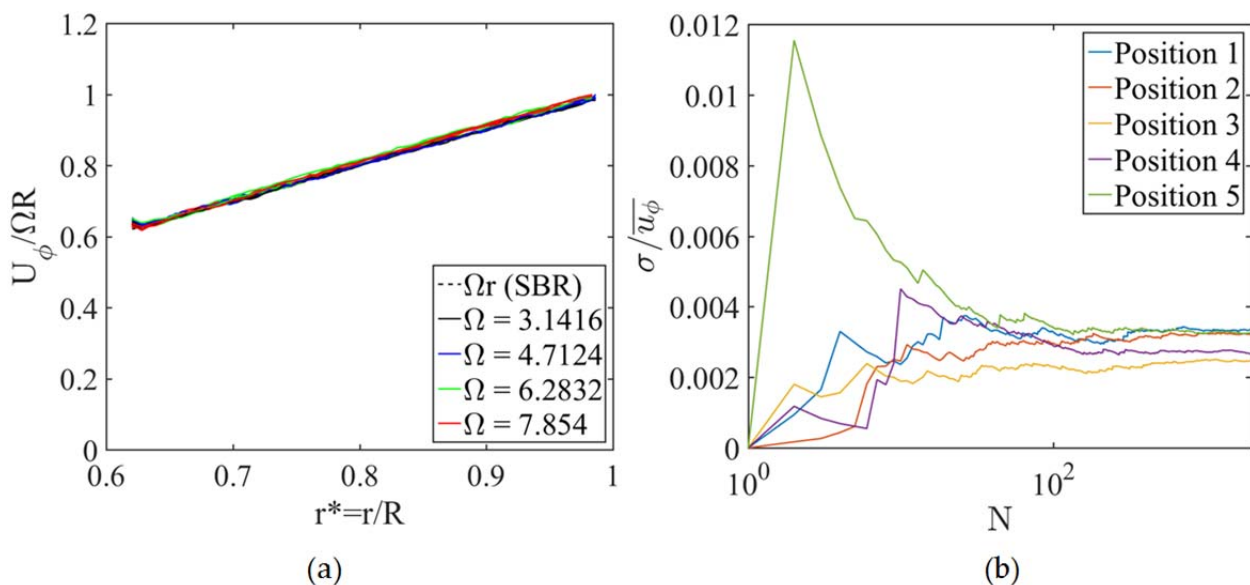


Fig. 4 (a) Normalized azimuthal velocity during SBR, (b) Convergence of the standard deviation at five points in the FOV (SBR, $\Omega = 4.7124$)

The small deviations are mainly caused by two effects. Besides the innate uncertainty of the measurement technique and its evaluation, the imaging process was performed phase locked in four positions per evolution. A not perfectly flat bottom wall of the cylinder may have introduced additional errors.

In addition to the absolute accuracy of the measurement process, transient problems should be evaluated in terms of reproducibility. The results of such a study indicate the dependence of a flow on imperfect initial conditions and other potential flaws of the experimental setup. Five measurements were performed for spin-up and spin-down at a spin rate of $\Omega = 2\pi f = 4.7124 \text{ s}^{-1}$.

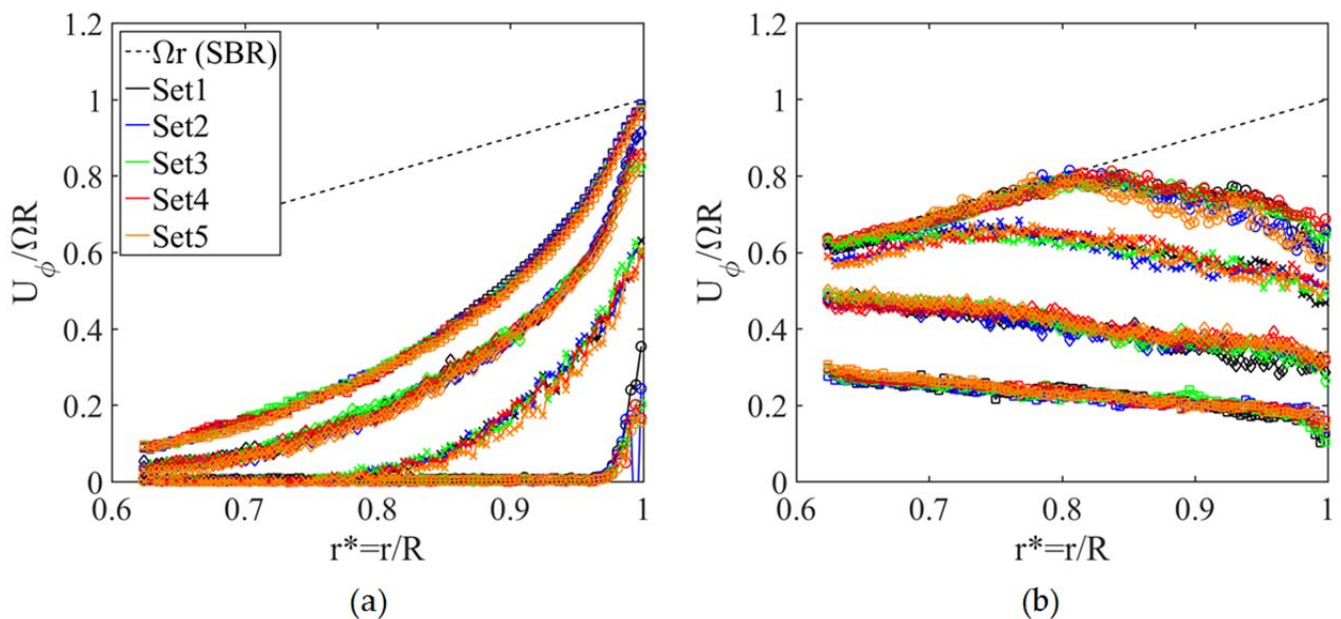


Fig. 5 Temporal development of azimuthal velocity (radial sample rate=50) at $t^*=13$ (o), 25(x), 64(\diamond) and 188(\square) for spin-ups (a) and spin-downs (b) of repeated measurements

Figure 5 shows the measured azimuthal velocities at four different time steps. Overall they show good agreement. In case of spin-down slight fluctuations are captured at $t^*=13$, which reduce with time, whose origin is discussed in the following.

To minimize the influence of bottom and top-wall effects, the measurement plane was positioned at $H/2$. Nonetheless, the sensitivity of the flow features towards the axial position was investigated by measuring spin-ups and spin-downs at $H/3$ and comparing it to the results of the $H/2$ -plane. Figure 6 provides the comparison for $\Omega = 2\pi f = 4.7124 \text{ s}^{-1}$. As clearly evident the measured velocity profiles are broadly similar, leading to the conclusion that the observed effects are not strongly influenced by end the bottom wall in the considered axial positions.

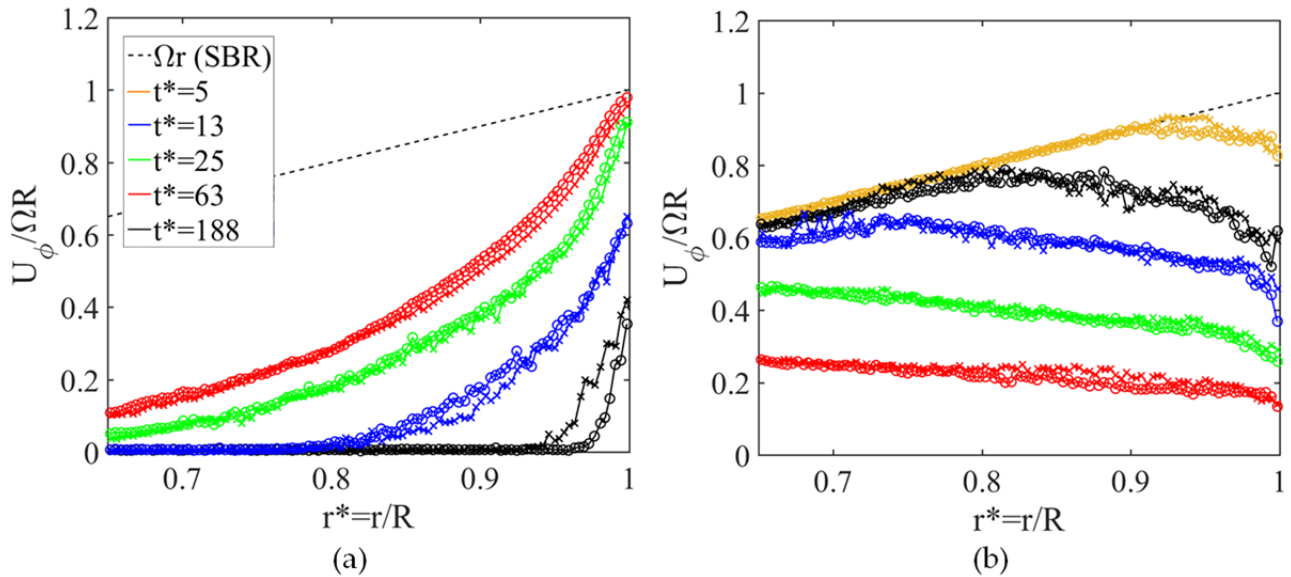


Fig. 6 Comparison of the azimuthal velocity profile for two measuring planes; (a) Spin-up and (b) Spin-down

4. Results

Experiments were performed at four different rotational speeds. The tank was spun up to 0.5, 0.75, 1.0 and 1.25 revolutions per second, resulting in angular velocities of $\Omega = 2\pi f = 3.14 \dots 7.854 \text{ s}^{-1}$ and Reynolds numbers in the range from $Re = 1.8 \cdot 10^5$ to $Re = 4.7 \cdot 10^5$. After the SBR was fully established the tank was stopped impulsively. Both, the spin-up and the spin-down process were captured. This section provides the results in terms of azimuthal velocity profiles, boundary layer growth and vorticity propagation. The observed phenomena are compared to numerical studies, which retroactively facilitate the understanding of the observed flow. Finally, the evaluation of the stereo PIV delivers insights into the axial velocity component.

The information over the whole measurement area was collapsed onto a virtual one-dimensional problem in radial direction. The azimuthal velocity profiles during spin-ups and spin-downs are shown in Figure 7 for different rotational speeds. Spin-ups show a characteristic diffusive profile similar to Stokes' first problem. Underlying mechanisms like Ekman pumping were expected to modify the time scale of the problem. However, the interaction with the free surface reduces the influence of the Ekman layer as the surface deformation counteracts the introduced convection. The slight variations of the profiles for different rotational speeds might be associated with the change in Froude numbers (O'Donnell and Linden, 1991).

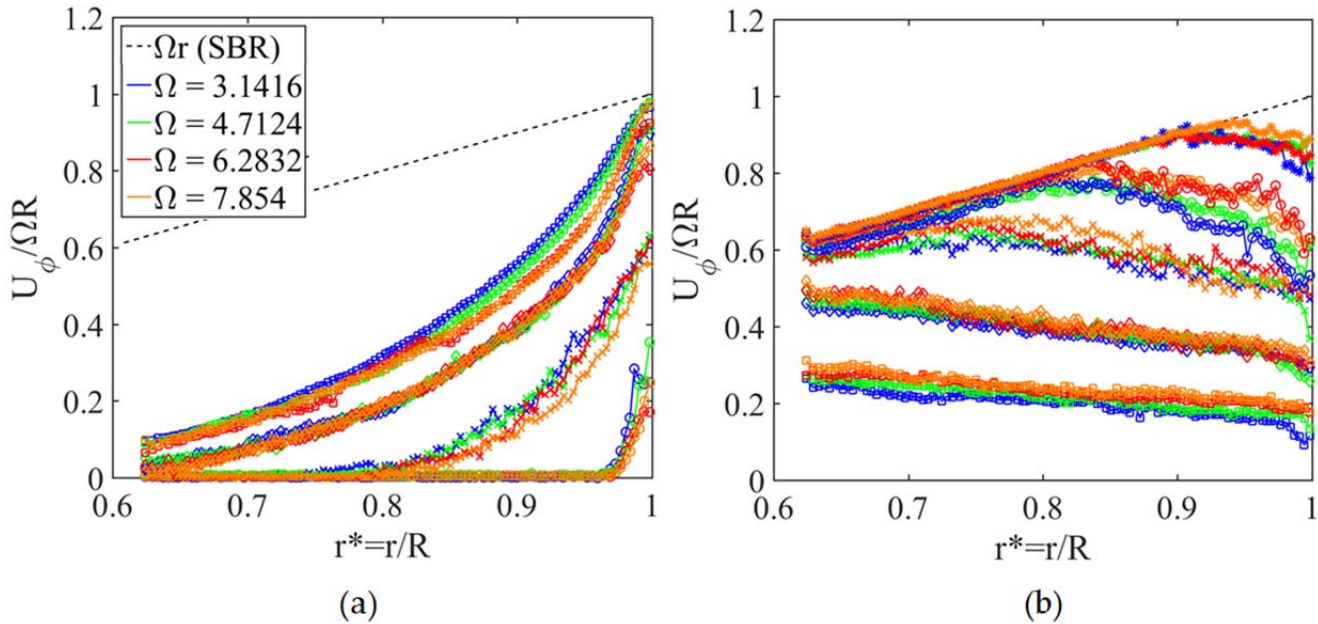


Fig. 7 Temporal development of the azimuthal velocity (radial sample rate=50= at $t^*=5(^*)$, 13(o), 25(x), 64(\diamond) and 188(\square) for (a) spin-ups and (b) spin-downs

In contrast, the velocity profiles during spin-down (Figure 7(b)) vary tremendously from the spin-up case. The information travels much faster towards the center of the tank and in the early stages of the spin-down large fluctuations occur between the different measurements.

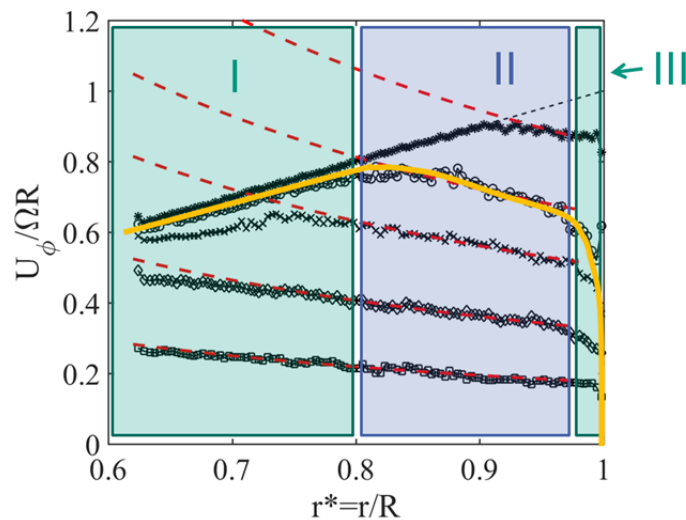


Fig. 8 Measured velocity profiles for $\Omega = 4.7124 \text{ s}^{-1}$ (black), velocity profiles of potential vortices ($\sim 1/r$, red), three distinct profile regions for $t^*=13$ (azimuthal velocity highlighted in yellow)

Three distinct regions can be differentiated from the centerline towards the wall. First, as shown in Figure 8, the SBR persists in the core and retracts quickly (Region I). Outside of that solid body core an almost irrotational velocity profile akin to a potential vortex occurs, representing

Region II. The measurement quality degenerates near the wall. Thus, the large velocity gradients in the boundary layer could not be measured. However, due to the no slip condition at the wall they must exist and can be declared as Region III.

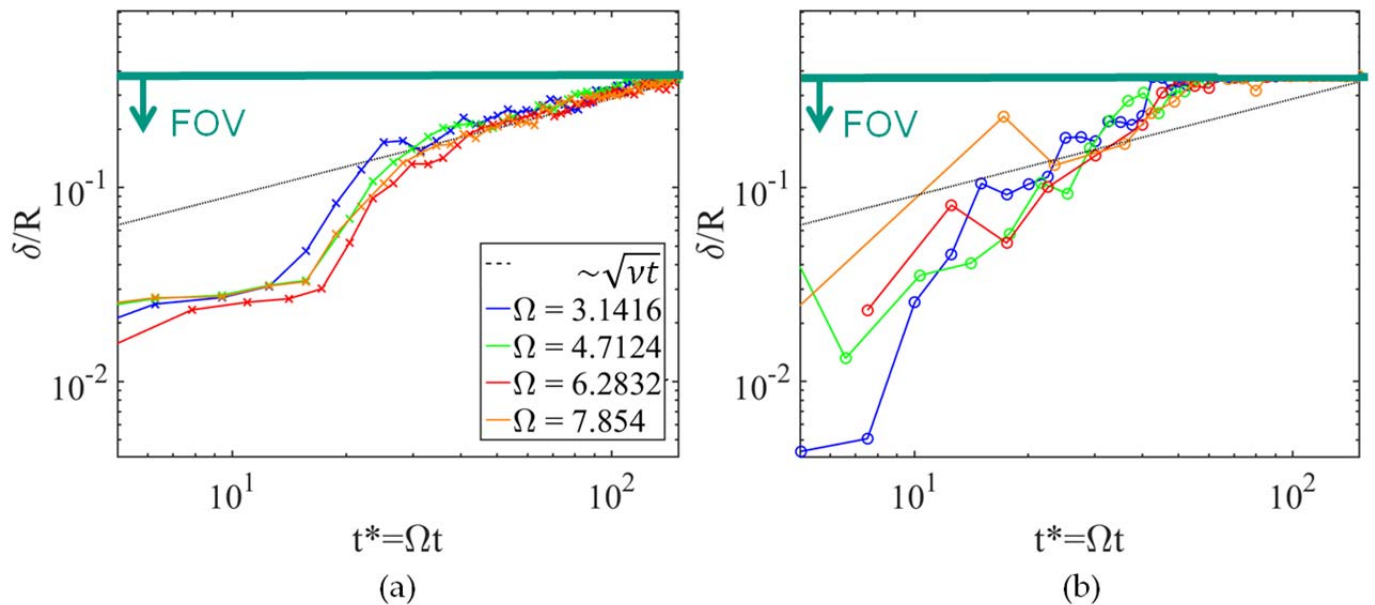


Fig. 9 Boundary Layer thickness for (a) spin-up and (b) spin-down

To analyse the propagation speed of information the boundary layer thickness is evaluated in case of spin-up and spin-down, respectively. A 2% deviation of the initial condition (averaged over 10 radial points) is defined as the boundary layer position δ (Figure 9). In case of spin-up the tank needs some time to accelerate to its final speed. From this point the boundary layer grows proportional to \sqrt{vt} . However, the spin-down occurs much faster and the SBR retracts from the FOV at $t^* \approx 60$.

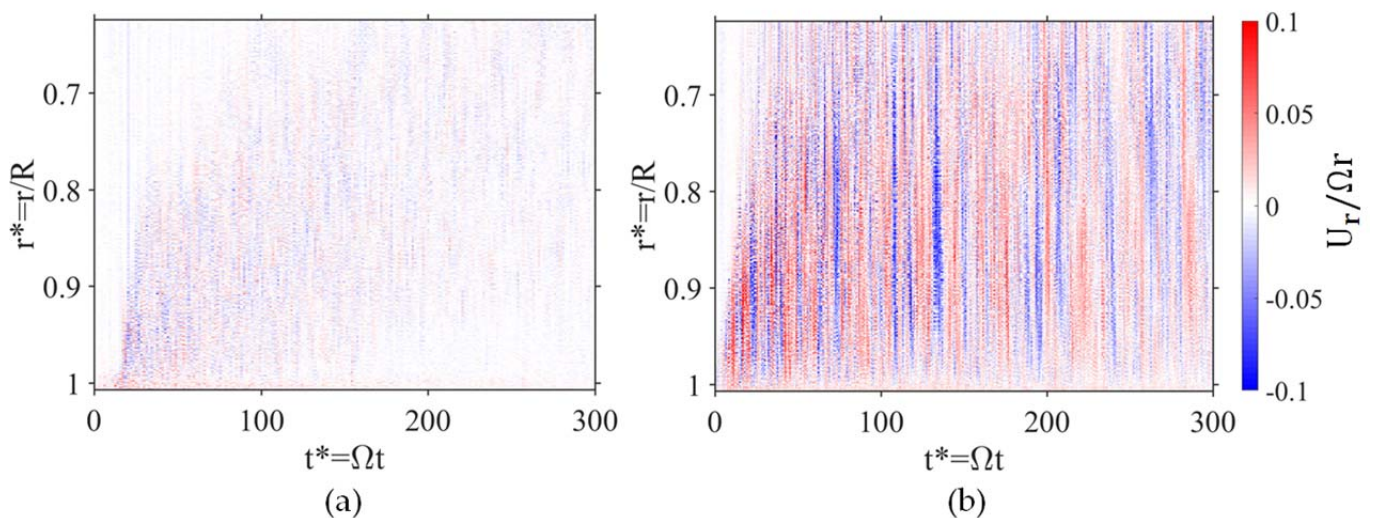


Fig. 10 Radial velocity development in case of (a) spin-up and (b) spin-down for $\Omega = 2\pi f = 4.7124 \text{ s}^{-1}$

The fast boundary layer growth paired with the deformation of the azimuthal velocity profile in case of spin-down points towards non-diffusive effects. Thus, the radial velocity component U_r is examined evaluated during spin-up and spin-down, respectively (see Figure 10). During spin-up, the radial velocity U_r is around two orders of magnitude smaller than the azimuthal velocity U_ϕ . Using this information and neglecting radial (and axial) velocities, the azimuthal component of the Navier-Stokes equation simplifies to

$$\frac{\partial U_\phi}{\partial t} = \nu \left(\frac{\partial}{\partial r} \left(\frac{U_\phi}{r} \right) + \frac{\partial^2 U_\phi}{\partial r^2} \right).$$

Only the viscous terms remain on the right side of the equation. Thus, just the initial and boundary conditions distinguish the spin-up from a Lamb-Oseen vortex, which emphasizes the diffusive time scale of the problem. However, during spin-down large and strongly fluctuating velocities occur in radial direction. The Rayleigh criterion for axisymmetric inviscid instabilities is obviously fulfilled in Region III and leads to the occurrence of instabilities and as a consequence to convective mixing and radial velocity components. Those instabilities retroactively explain the large fluctuations between different measurements during the onset of the spin-down process (see Figures 5(b) and 7(b)) as they cause complex turbulent three-dimensional flow structures, which deviate slightly for each run of the experiment.

Returning to the initial question of vorticity propagation, Region II in Figure 8 already pointed towards some interesting features of the spin-down case. The vorticity data is calculated with a least square differentiation scheme for oversampled data from Raffel et al. (2007). In addition it is filtered by a second-order Savitzky-Golay filter (Savitzky and Golay, 1964) with a timespan of $t^*=30$ to reduce measurement noise (Figure 11). In accordance with the boundary layer also the vorticity (induced at the side walls) travels faster into the tank in the case of spin-down. In both cases large amounts of vorticity are introduced at the side walls and propagate towards the middle of the tank. There are, however, fundamental qualitative differences concerning the area affected by the side walls. During spin-up a smooth radial decay of vorticity is detected (see Figure 11(a)). At some point in time, long after the end of the measurements, its diffusion leads to SBR. In the spin-down case no smooth diffusion of vorticity is detectable. The area affected by the change of the tank's angular velocity is (temporally averaged) free of vorticity (see Figure 11(b)).

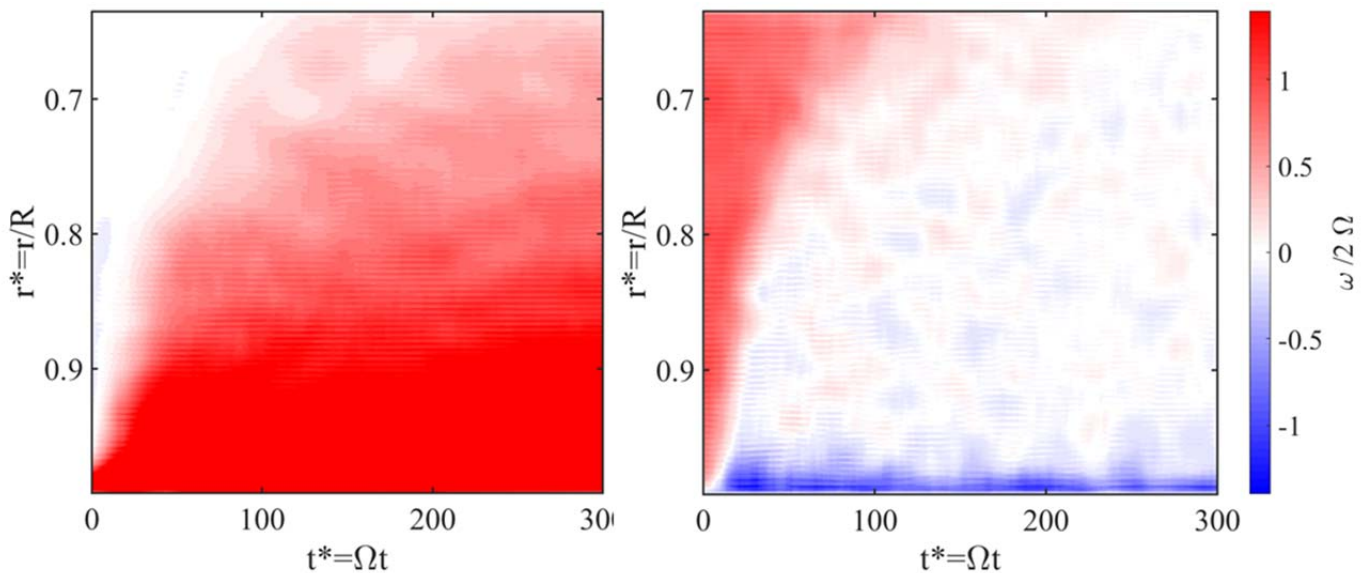


Fig. 11 Development of the vorticity in case of (a) spin-up and (b) spin-down for $\Omega = 4.7124 \text{ s}^{-1}$

To validate the experimental results and to gain a better understanding of the three-dimensional flow structures, occurring during spin-down, additional data was generated via direct numerical simulation (DNS) of axially-periodic turbulent pipe flow. Due to exploding computational costs with increasing Reynolds number, simulation have necessarily been performed at lower values of Re compared to the experiment ($Re = 3000$). The simulations have been run with the pseudo-spectral, parallel solver for the incompressible Navier-Stokes equations in cylindrical coordinates developed by M. Quadrio and P. Luchini (please refer to Luchini and Quadrio (2006) for the description of a similar code). The velocity is spatially discretized via Fourier expansion in axial and azimuthal direction and with sixth-order compact finite differences in radial direction. High efficiency is obtained through a variable number of azimuthal Fourier modes in the radial direction, so as to keep the spatial resolution constant.

The influence of disturbances in the initial flow field was tested by applying different disturbance setting on both, spin-up and spin-down, respectively. The spin-up case (not shown here) remained stable, independently from the disturbances in the initial conditions.

First, a disturbance free setting was realised. Figure 12(a) shows the development of the azimuthal velocity profiles. Due to the small Reynolds number and the hereby dominant viscous damping the undisturbed spin-down case remains stable, even though the magnitude of the circulation decreases in radial direction. The absence of convection limits the vorticity propagation to a diffusive time scale, answering the initial question about the annihilation and

propagation of vorticity for very small Reynolds numbers. In the non-convective case without instabilities, the introduced vorticity propagates at the same speed, independently on the initial vorticity field.

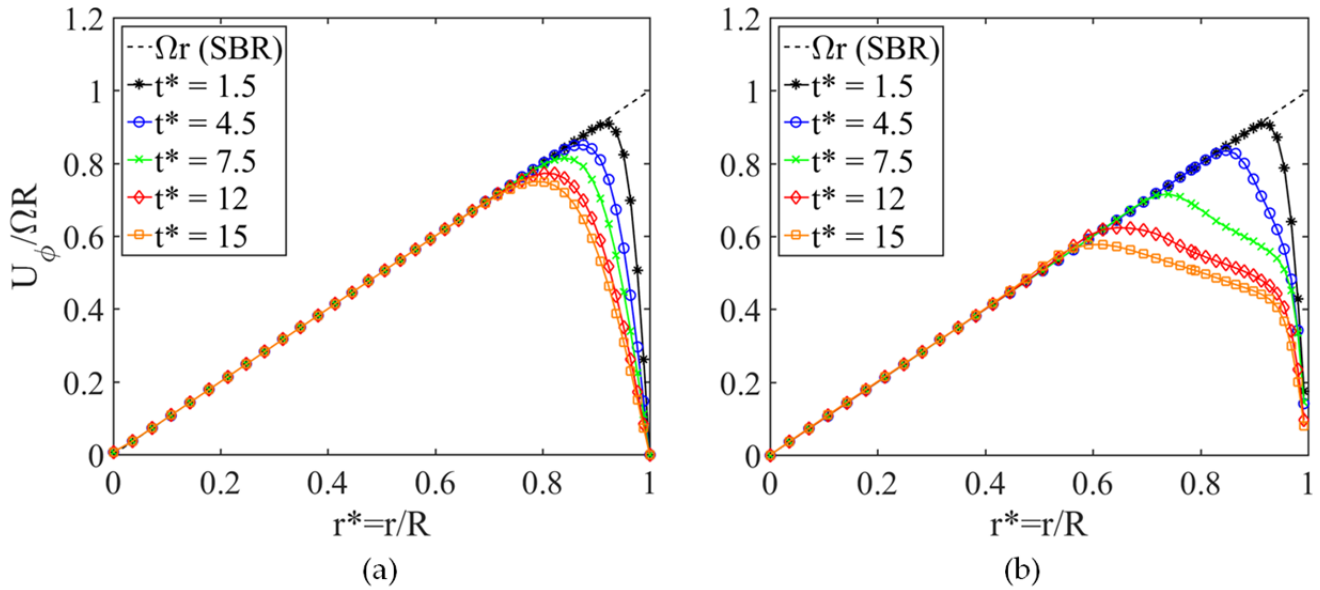


Fig. 12 DNS results of spin-down at $Re=3000$. (a) Completely undisturbed SBR, (b) SBR with small divergence free disturbances

As a second step very small disturbances ($U'_{max} \approx 10^{-6} \Omega R$) are added to the initial conditions. The satisfaction of the continuity equation was realised in two different ways. The easiest way to ensure a divergence free velocity field is to set each term of the continuity equation to 0

$$\frac{\partial(rU_r)}{\partial r} = 0; \quad \frac{\partial U_\phi}{\partial \phi} = 0; \quad \frac{\partial U_z}{\partial z} = 0.$$

Note that the disturbance of the azimuthal velocity remains axisymmetric in this setting. Additionally, a completely random distribution of the disturbances was implemented (still ensuring a divergence free velocity field). The resulting spatially averaged azimuthal velocity profiles were very similar for both cases. As expected, the disturbances are damped during spin-up and the boundary layer develops similar to the undisturbed case. However, radial convective flows, introduced by instabilities, deform the azimuthal velocity profile in case of spin-down (see Figure 12(b)). After initial time steps, where the boundary layer development is still driven by viscosity, convection sets in and leads to velocity profiles similar to the measured data shown in Figure 7 and 8. The delay before the onset of radial influx was not captured during the experiments as, due to the much higher Reynolds number, it occurred instantly.

The convective flows are further visualised by means of Lagrangian Coherent Structures (LCS); see e.g. Haller and Yuan (2000) and Shadden et al. (2005). Attracting LCS, extracted by means of the Finite-time Lyapunov exponent (FTLE), are able to draw a distinct separating surface between particles in the core of the SBR and particles coming from the side walls. This allows neat three-dimensional visualization of the complex flows evolving during spin-down. The instabilities at the side walls cause radial jets, which are deflected upwards and downwards by the inner fluid of the SBR. As already observed by Euteneuer (1972) and Neitzel and Davis (1981) this results in growing counter rotating Görtler vortices at the side walls. In case of axisymmetric disturbances of the azimuthal velocity profile the evolving jets and vortices are also axisymmetric (see Figure 13). However, the completely random disturbances result in non-axisymmetric flow structures, which strengthen in time and even lead to detachment from the wall. While, the basic features of deflected radial jets and the growing streamwise vortices remain similar to the axisymmetric case, the evolving structures are much more complex.

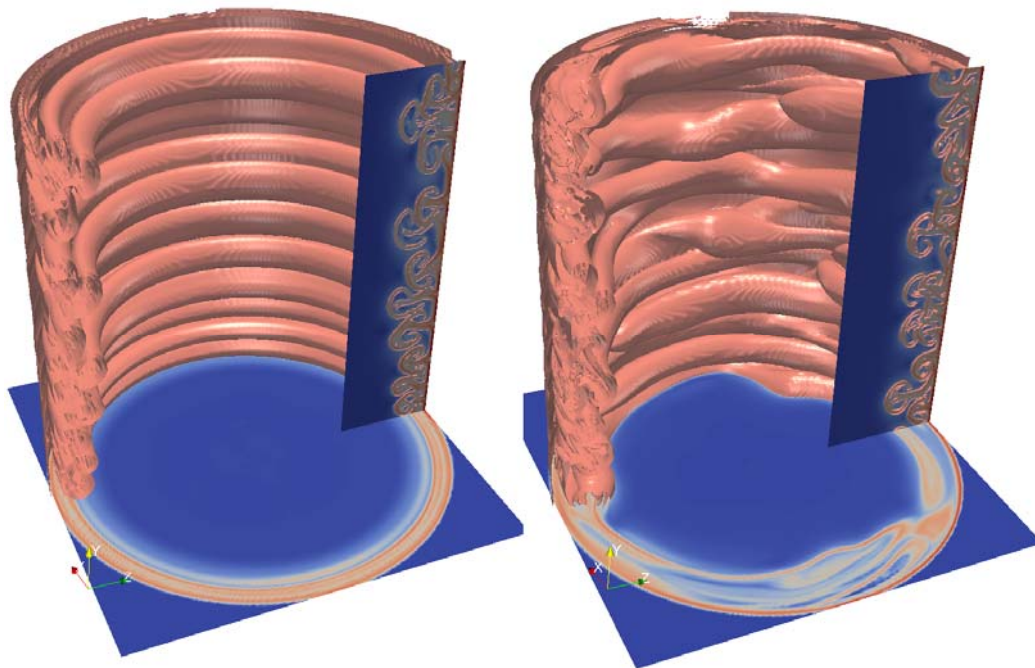


Fig. 13 Attracting LCS in DNS results of spin-down at $Re=3000$ at $t^*=6.5$. Axisymmetric disturbances on initial condition. (left), Non-axisymmetric disturbances on initial condition (right)

To check on the symmetry of the occurring instabilities in the actual experiment, stereo PIV measurements were performed as described in Section 2. As Görtler vortices grow in time, their relative position towards the measuring plane varies (see Figure 14(a)). Therefore, not every measured velocity field contains out of plane velocities triggered by Görtler vortices. Figure

14(b)-(d) provides the axial velocity at several time steps, where the Görtler vortices are coincidentally in the measuring plane. As discussed, they grow over time. Additionally, the non-axisymmetric behaviour predicted by the DNS is detected. The magnitude of the out of plane component decreases in time. This points towards an interesting feature of the spin-down phenomenon. The impulsive spin-down instantly evokes large velocity gradients at the side walls, which result in fast radial jets and thus in strong Görtler vortices. However, those velocity gradients decrease very fast due to the strong mixing. This in turn leads to weaker jets and the driving force of the Görtler vortices is reduced.

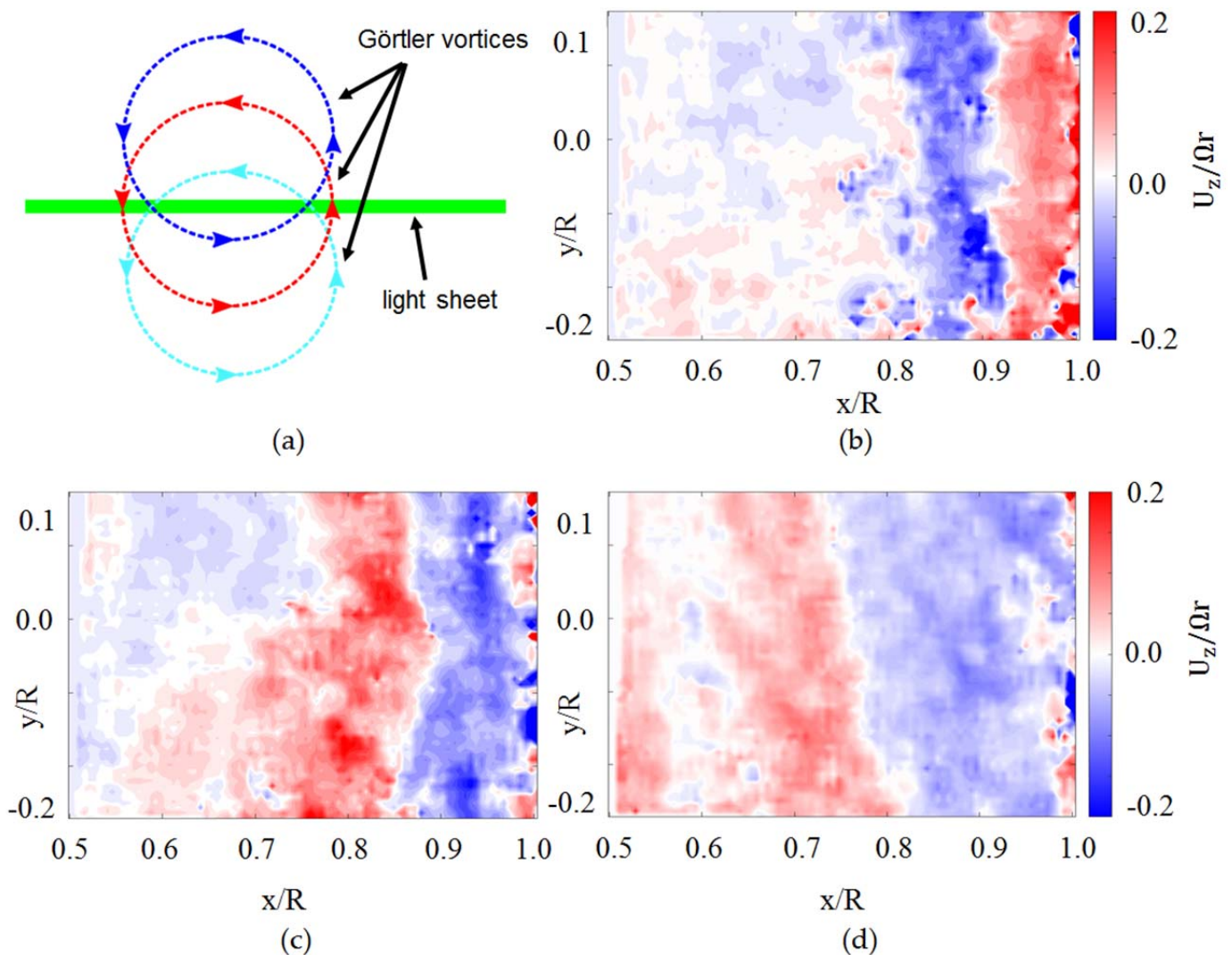


Fig. 14 (a) Görtler vortex light sheet interaction, axial velocities at (b) $t^*=18$, (c) $t^*=24$, (d) $t^*=91$

The declining radial jets could lead to a slower boundary layer growth as soon as the gradients in the near wall region decrease. As the experimental data does not capture the complete development process of the boundary layer due to the limited FOV, again the numerical data is evaluated. Figure 15 shows the boundary layer growth in the numerical simulations by means of

a 2% deviation of the SBR. After the diffusive onset of the spin-down the convective mixing significantly speeds up the process. However, finally the boundary layer again grows at a smaller time scale.

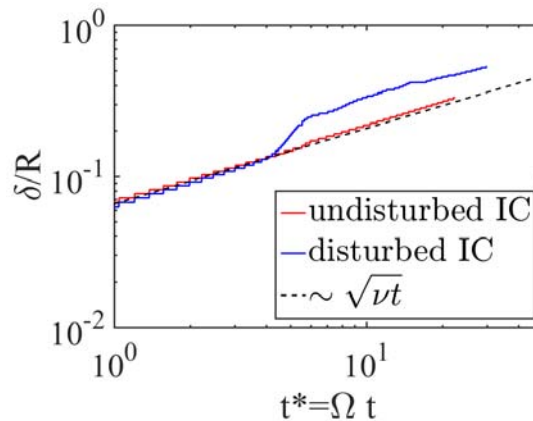


Fig. 15 Boundary Layer thickness in the numerical data (spin-down)

5. Concluding Remarks

The study shows the anticipated behaviour that is typical of spin-up and spin-down situations in rotating tanks. The measurement setup was proven to be appropriate to successfully deliver measurements with small error margins. As a result, it was found that the spin-up case behaves similar to an inverse Lamb-Oseen vortex. On the other hand, spin-down has shown significantly different behaviour, which is found to be related to instabilities. Three distinct regions can be identified in the azimuthal velocity profile: a retracting SBR core, a region containing Görtler vortices and a vorticity-feeding near wall region with a large velocity gradient. In the intermediate region, the mixing induced by the instability-driven Görtler vortices causes the local axial vorticity field to be zero (apart from small fluctuations) and thus the velocity profile to be similar to a potential vortex. This can be affiliated to the Rayleigh criterion, which establishes that a vorticity free zone is the minimum criterion for stability in a rotating flow. Thus, the inherently unstable spin-down process forms an azimuthal velocity profile similar to a potential vortex to meet the stability requirement. As a consequence, the occurring Görtler vortices, which cause a rapid exchange of high and low momentum fluid, speed up the annihilation of vorticity. This in turn answers the original question: initial- and boundary conditions do play a role in the behaviour of vorticity annihilation and propagation (apart from flows with very small Reynolds numbers).

There remain open questions which will be addressed in future work. The momentum of the radial jets and its influence on the vorticity propagation is of interest. Furthermore, the scaling for even larger Reynolds numbers will be considered in upcoming experiments in both, the test rig in Karlsruhe and at the rotating CORIOLIS platform in Grenoble. In parallel, further numerical investigations will cover the range of small to medium Reynolds numbers and hopefully provide deeper insights into the complex three-dimensional flow structures.

6. References

- Benton ER, Clark A (1974) Spin-Up. *Annual Review of Fluid Mechanics* 6 (1) 257–280. doi:10.1146/annurev.fl.06.010174.001353.
- Cederlöf U (1981) Free-surface effects on spin-up. *Journal of Fluid Mechanics* 187 (-1) (1988) 395. doi:10.1017/S0022112088000485.
- Duck, PW, Foster MR (2001) Spin-up of homogeneous and stratified fluids. *Annual review of fluid mechanics* 33.1: 231-263.
- Euteneuer GA (1972), Die Entwicklung von Längswirbeln in zeitlich anwachsenden Grenzsichten an konkaven Wänden. *Acta Mechanica* 13 (3-4) 215–223.
- Greenspan HP, Howard LN (1963), On a time-dependent motion of a rotating fluid. *Journal of Fluid Mechanics* 17 (03) (1963) 385. doi:10.1017/S0022112063001415.
- Haller G, Yuan G (2000) Lagrangian coherent structures and mixing in two-dimensional turbulence. *Physica D: Nonlinear Phenomena* 147.3 (2000): 352-370.
- Kriegseis J, Kinzel M, Rival DE (2013) On the persistence of memory: do initial conditions impact vortex formation? *Journal of Fluid Mechanics* 736, 91–106. doi:10.1017/jfm.2013.528.
- Luchini P, Quadrio M (2006) A low-cost parallel implementation of direct numerical simulation of wall turbulence. *Journal of Computational Physics* 211.2: 551-571.
- Neitzel GP, Davis SH (1981), Centrifugal instabilities during spin-down to rest in finite cylinders. numerical experiments. *Journal of Fluid Mechanics* 102 329–352. doi:10.1017/S002211208100267X.
- O'Donnell J, Linden PF (1991), Free-surface effects on the spin-up of fluid in a rotating cylinder. *Journal of Fluid Mechanics* 232 (-1) 439. doi:10.1017/S0022112091003762.
- Raffel M, Willert C, Wereley S, Kompenhans J (2007), *Particle image velocimetry: a practical guide*. 2nd Edition, Springer

Rayleigh L (1917) On the dynamics of revolving fluids. Proceedings of the Royal Society of London. Series A, Containing Papers of a Mathematical and Physical Character 93.648: 148-154.

Saric WS (1994) Görtler Vortices. Annual Review of Fluid Mechanics 26 (1) 379–409.
doi:10.1146/annurev.fl.26.010194.002115.

Savitzky A , Golay MJE (1964) Smoothing and differentiation of data by simplified least squares procedures. Analytical chemistry 36.8: 1627-1639.

Shadden SC, Lekien F, Marsden JE (2005) Definition and properties of Lagrangian coherent structures from finite-time Lyapunov exponents in two-dimensional aperiodic flows. Physica D: Nonlinear Phenomena 212.3 (2005): 271-304.

Taylor GI (1923) Stability of a viscous liquid contained between two rotating cylinders. Philosophical Transactions of the Royal Society of London. Series A, Containing Papers of a Mathematical or Physical Character 223: 289-343.

Wedemeyer EH (1964) The unsteady flow within a spinning cylinder. Journal of Fluid Mechanics 20.03: 383-399.

Westerweel J, Scarano F (2005), Universal outlier detection for PIV data. Experiments in Fluids 39 (6) 1096–1100. doi:10.1007/s00348-005-0016-6.